

# The Influence of Nonstationary Carrier Transportation the Bandwidth of p-i-n Photodiode

Petar S. Matavulj, Dejan M. Gvozdić, and Jovan B. Radunović

**Abstract**—The influence of nonstationary carrier transport on the bandwidth and the bandwidth-quantum efficiency product of p-i-n photodiodes is analyzed using the complete phenomenological model for two-valley semiconductors. The analysis has been made for various submicron and micron dimensions, for different bias voltages and for several energies of incident pulse excitation, including the variation of the active area of the p-i-n photodiode. The analysis shows that, as the thickness of the absorption layer varies, the bandwidth could have more than one maximum, especially for smaller bias voltages. The optimal thickness of the absorption layer versus bias voltage and device area is determined, providing maximal bandwidth and maximal bandwidth-quantum efficiency product.

**Index Terms**—Charge carrier processes, integrated optoelectronics, optical communication, p-i-n photodiodes, semiconductor device modeling.

## I. INTRODUCTION

THE photodetectors bandwidth is one of the most critical factors for new high bit rate optical communication systems. Many papers deal with the bandwidth or frequency response of p-i-n photodiodes. In a number of these papers, models of p-i-n photodetector and the transport equations of photogenerated carriers are based on many questionable assumptions.

Lucovsky [1] calculated the frequency response of the silicon p-i-n photodetectors by solving linear equations for the carrier concentrations and photocurrent density in the intrinsic region of the p-i-n photodiode, assuming constant values for carrier velocities. The expression of the frequency response provided in [1] by Lucovsky cannot be used for two-valley semiconductor devices, because the velocities in these semiconductors cannot be assumed constant, due to their considerable variation with the applied electric field.

Bowers *et al.* [2] estimated the detector bandwidth, by assuming that in high electric fields (above 50 kV/cm) all carriers travel at the saturation velocity. This estimate is good for thin absorption layers (submicron dimension) and in the case of RC-limited bandwidth, but is not quite correct for larger absorption layer thickness (micron dimension) and for transit time limited bandwidth.

Sabella *et al.* [3] presented an analytical model of an InGaAs p-i-n photodetector, operating up to moderate illumination

intensities. This model does not properly take into account the influence of the RC constant on the bandwidth.

Dentan *et al.* [4] have studied the nonlinear response of p-i-n InGaAs photodiode, induced by space charge effects due to photogenerated carriers. However, this paper does not take into account nonstationary effects caused by electron intervalley transfer, that can influence the bandwidth even for absorption layer thickness in the micron range.

The nonstationary and nonlinear response of a p-i-n photodiode made of a two-valley semiconductor has been studied in [5]. However, this paper analyzed the nonlinearity but neglected the change of the bias voltage and the influence of the RC-constant.

In this paper, the bandwidth of p-i-n GaAs photodiode is analyzed, using an extended phenomenological model of transport equations [5]. This model is able to take into account the change of the electric field caused by space charge of photogenerated carriers and also the influence of bias voltage variation and nonstationary effects caused by electron intervalley transfer. The complete phenomenological model of transport equations allows for electron intervalley transfer, which can be very important in submicron and micron devices [6]. Using this model, we show that, as the thickness of the absorption layer varies, the bandwidth can have more than one maximum, particularly for lower bias voltages and low energies of the incident pulse. These optimal thicknesses depend on the RC-constant (active area of the photodiode and the load resistance) and values of the bias voltage.

## II. THE MODEL

We consider a p-i-n photodiode, made of a two-valley semiconductor (GaAs). The photodiode structure is shown in Fig. 1(a).

The electric circuit of the photodiode, used for detection, is shown in Fig. 1(b). The detected signal is denoted as  $U_R(t)$ ,  $U(t)$  is the voltage of the reverse biased p-i-n photodiode,  $I(t)$  is its photocurrent, and  $R$  the load resistance. In the photodiode equivalent circuit, the resistance of the diode contacts and the parasitic capacitance of the external circuit are neglected, while the p-i-n photodiode capacitance is taken into account via the displacement current. During the detection of the incident radiation, the photodiode generates a photocurrent that causes a voltage drop on the load resistance, thus changing the photodiode voltage

$$U(t) = V_{cc} - RI(t). \quad (1)$$

Manuscript received August 14, 1996; revised August 4, 1997.

The authors are with the Faculty of Electrical Engineering, Belgrade University, Belgrade 11000 Yugoslavia.

Publisher Item Identifier S 0733-8724(97)08893-2.

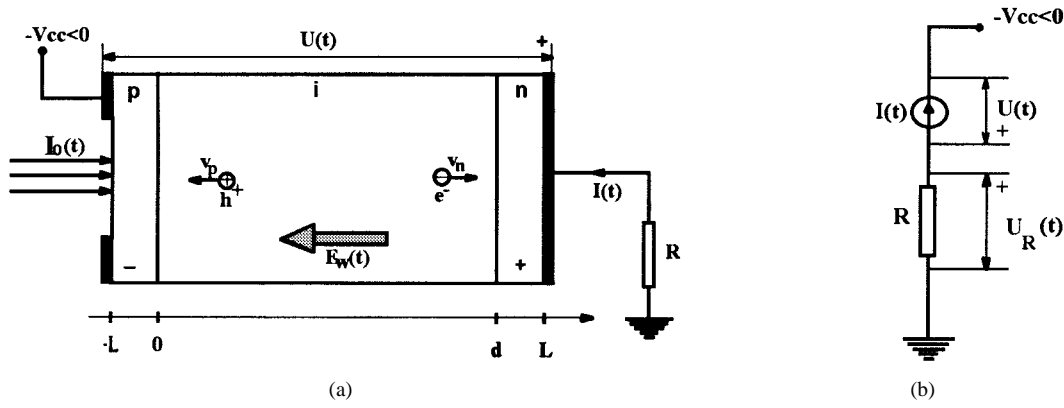


Fig. 1. The structure of the p-i-n photodiode and the equivalent electric circuit.

This causes a perturbation of the electric field controlling the carriers transport, inducing change of carriers transit time and change of the bandwidth.

The electric field has two components, one being the electric field  $E_W(x, t)$  in the case of weak optical generation and the other is the space-charge induced field  $E_{SC}(x, t)$ . The first component of the electric field is determined by the concentration of fixed charges and the variable reverse-bias voltage, and the second component by the concentration of photogenerated carriers. The electric field in the i-region is shown in (2)–(4) at the bottom of the page where  $d$  is the width of the i-region,  $L$  and  $L$  are the widths p- and n-regions, respectively.

$$V_D(d) = \frac{eNd^2}{2\epsilon}$$

is the punchthrough voltage ( $N$  is the small residual donor concentration in the absorption layer;  $P^+$  and  $N^+$  are acceptor and donor concentrations in p- and n-regions, respectively)

$$w(t) = \sqrt{\frac{2\epsilon U(t)}{eN}}$$

is the width of depletion layer.  $\epsilon = \epsilon_0\epsilon_r$  is the dielectric constant of GaAs and  $e$  the electron charge. Subscripts 1 and 2 correspond to electrons in the conduction-band valley (1) (the central valley) and the conduction-band valley (2) (the satellite valleys).

To analyze the detection process in the two-valley semiconductor we have to use the transition rates for intervalley electron transfer in the continuity equations for the central and the satellite valley electrons. The continuity equations for

electrons and holes read

$$\frac{\partial n_1(x, t)}{\partial t} - \frac{1}{e} \frac{\partial}{\partial x} j_1(x, t) = G_{op}(x, t) + g(x, t) \quad (5)$$

$$\frac{\partial n_2(x, t)}{\partial t} - \frac{1}{e} \frac{\partial}{\partial x} j_2(x, t) = -g(x, t) \quad (6)$$

$$\frac{\partial p(x, t)}{\partial t} + \frac{1}{e} \frac{\partial}{\partial x} j_p(x, t) = G_{op}(x, t). \quad (7)$$

They should be solved together with the drift-diffusion equations for the optically generated electrons

$$j_i(x, t) = en_i(x, t)v_i(x, t) + e \frac{\partial}{\partial x} (D_i n_i(x, t)), \quad i = 1, 2 \quad (8)$$

$$j_n(x, t) = j_1(x, t) + j_2(x, t) \quad (9)$$

and with the corresponding the drift-diffusion equations for optically generated holes

$$j_p(x, t) = ep(x, t)v_p(x, t) - e \frac{\partial}{\partial x} (D_p p(x, t)). \quad (10)$$

Thus, the total conduction current density equals

$$j(x, t) = j_n(x, t) + j_p(x, t). \quad (11)$$

$D_1$ ,  $D_2$  i  $D_p$  are diffusion constants for electrons in the central and the satellite valleys and for holes, respectively.

The net transfer rate is given by

$$g(x, t) = \frac{n_2(x, t)}{\tau_{21}(E(x, t))} - \frac{n_1(x, t)}{\tau_{12}(E(x, t))} \quad (12)$$

where  $\tau_{12}(E(x, t))$  and  $\tau_{21}(E(x, t))$  are the phenomenological values of electron transfer times from valley (1) to valley (2) and *vice versa* [5], [6].

$$E(x, t) = E_W(x, t) + E_{SC}(x, t) \quad (2)$$

$$E_W(x, t) = \begin{cases} -\frac{eN}{\epsilon}(w(t) - x), & 0 \leq x \leq w(t) \quad (\text{for } w(t) \leq d) \\ -\frac{eN}{\epsilon}(d - x) - \frac{U(t) - V_D(d)}{d}, & 0 \leq x \leq d \quad (\text{for } w(t) > d) \\ 0, & \begin{cases} -L \leq x \leq 0 \text{ and } d < x \leq L \\ \text{and} \\ (w(t) < x \leq d \text{ for } w(t) \leq d) \end{cases} \end{cases} \quad (3)$$

$$\frac{\partial E_{SC}(x, t)}{\partial x} = \frac{e}{\epsilon}(p(x, t) - n_1(x, t) - n_2(x, t)) \quad (4)$$

In the above equations we neglect recombination, because we assume that the processes considered are fast. We also neglect thermal generation, because it creates the dark current that is negligible when compared to the photocurrent throughout the range of investigation.

The pulsed optical generation rate is

$$G_{\text{op}}(x, t) = \alpha I_0(t) e^{-\alpha x} \quad (13)$$

where  $I_0(t)$  is the incident photon flux density

$$I_0(t) = \frac{W}{\lambda S} \delta(t) = I_0 \delta(t)$$

with  $W$  being the energy of incident light,  $\lambda$  the wavelength of incident light,  $S$  the p-i-n photodiode active area,  $h$  Planck's constant,  $c$  the velocity of light, and  $\alpha$  is the optical absorption coefficient of GaAs.

The velocity versus electric field dependence was taken from [7]

$$v_i(x, t) = \begin{cases} \mu_i E(x, t), & v_i(x, t) \leq v_{is} \\ v_{is}, & \text{otherwise} \end{cases}, \quad i = 1, 2 \quad (14)$$

where  $v_{1s}$  and  $\mu_1$  are the saturation velocity and mobility of electrons in the central valley, respectively, and  $v_{2s}$  and  $\mu_2$  the corresponding quantities in the satellite valleys, respectively. Similarly, for holes we have

$$v_p(x, t) = \begin{cases} \mu_p E(x, t), & v_p(x, t) \leq v_{ps} \\ v_{ps}, & \text{otherwise} \end{cases} \quad (15)$$

where  $v_{ps}$  and  $\mu_p$  are the saturation velocity and mobility of holes, respectively.

The p-i-n photodiode response is given by the relation [5]

$$I(t) = \frac{S}{d} \int_0^d j(x, t) dx + \frac{\varepsilon S}{d} \frac{dU(t)}{dt}. \quad (16)$$

The first term in the above equation is the conduction current, and the second term is the displacement current.

Equations (1)–(16) together with the initial conditions

$$\begin{aligned} n_1(x, 0) &= p(x, 0) = \alpha I_0 e^{-\alpha x} \\ n_2(x, 0) &= 0 \\ E(x, 0) &= E_W(x, 0) \\ U(0) &= V_{\text{CC}} \end{aligned} \quad (17)$$

and boundary conditions [5]

$$\begin{aligned} n_1(-\mathbf{L}, t) &= n_1(L, t) = 0 \\ n_2(-\mathbf{L}, t) &= n_2(L, t) = 0 \\ p(-\mathbf{L}, t) &= p(L, t) = 0 \end{aligned} \quad (18)$$

make a closed system that enables one to determine the current response, i.e., the change of the photodiode voltage during detection.

TABLE I  
PARAMETERS OF THE p-i-n PHOTODIODE CONSIDERED

|                 |   |           |   |                 |   |
|-----------------|---|-----------|---|-----------------|---|
| $p^+$           | $= 10^{19} \text{ cm}^{-3}$                               | $N$       | $= 10^{14} \text{ cm}^{-3}$   | $N^+$           | $= 10^{17} \text{ cm}^{-3}$                           |
| $\mathbf{L}$    | $= 0.1 \text{ } \mu\text{m}$                              | $d$       | $= \begin{cases} 0.1 \\ \vdots \\ 5 \end{cases} \text{ } \mu\text{m}$     | $L$             | $= 0.1 \text{ } \mu\text{m}$                          |
| $\alpha$        | $= 10^4 \text{ cm}^{-1}$                                  | $\lambda$ | $= 0.8 \text{ } \mu\text{m}$  | $\varepsilon_r$ | $= 11.36$   |
| $\mu_1$         | $= 7500 \frac{\text{cm}^2}{\text{Vs}}$                    | $\mu_2$   | $= 50 \frac{\text{cm}^2}{\text{Vs}}$                                      | $\mu_p$         | $= 420 \frac{\text{cm}^2}{\text{Vs}}$                 |
| $v_{1s}$        | $= 10^8 \frac{\text{cm}}{\text{s}}$                       | $v_{2s}$  | $= 10^7 \frac{\text{cm}}{\text{s}}$                                       | $v_{ps}$        | $= 5 \times 10^6 \frac{\text{cm}}{\text{s}}$          |
| $D_1$           | $= 970 \frac{\text{cm}^2}{\text{s}}$                      | $D_2$     | $= 8.6 \frac{\text{cm}^2}{\text{s}}$                                      | $D_p$           | $= 18.2 \frac{\text{cm}^2}{\text{s}}$                 |
| $R$             | $= 50 \text{ } \Omega$                                    | $S$       | $= \begin{cases} 70 \\ \vdots \\ 5000 \end{cases} \text{ } \mu\text{m}^2$ | $W$             | $= \begin{cases} 0.002 \\ 0.1 \end{cases} \text{ pJ}$ |
| $V_{\text{CC}}$ | $= \begin{cases} 2 \\ \vdots \\ 20 \end{cases} \text{ V}$ |           |   |                 |   |

### III. PARAMETERS OF CALCULATION AND NUMERICAL TECHNIQUES

The analysis of transport processes in the photodiode is performed using the parameters given in Table I.

The system of (1)–(18) was solved by the method of finite differences, observing the stability condition  $v_{\text{max}} \Delta t \leq \Delta x$  [8], where  $v_{\text{max}} = v_{1s}$  is the maximum carrier velocity. The spatial step  $\Delta x$  was chosen from this condition, while  $\Delta t = 10^{-4}$  ps is adopted for the time step. The bandwidth frequency is calculated using the fast Fourier transform, applied to the current response. The bandwidth-quantum efficiency product is presented as a product of calculated bandwidth and  $\eta$ , given by

$$\eta = (1 - e^{-\alpha d}). \quad (19)$$

### IV. RESULTS AND DISCUSSION

Fig. 2 depicts the dependence of the bandwidth on the thickness of the absorption region of p-i-n photodiode together with the transit time limited bandwidth. The bandwidth calculations were performed for the bias voltage  $V_{\text{CC}} = 5$  V, active area of  $S = 700 \text{ } \mu\text{m}^2$  and two values of the incident excitation energy  $W = 0.002$  pJ and  $W = 0.1$  pJ. The incident excitation energy may be expressed via the ratio of the maximal concentration of photogenerated carriers and the donor concentration in the absorption layer ( $\gamma$ ), that may be called the excitation level. For  $W = 0.002$  pJ this ratio is  $\gamma = 0.1$  and for  $W = 0.1$  pJ it is  $\gamma = 5$ . Fig. 2 shows that, for bias voltage higher than 5 V and  $\gamma$  lower than five, the influence of the space charge on the bandwidth is practically negligible.

In case of submicron dimensions an increase of the absorption layer thickness causes a linear increase of the bandwidth. For micron dimensions, however, the bandwidth decreases as the absorption layer depth increases. It can be seen that the

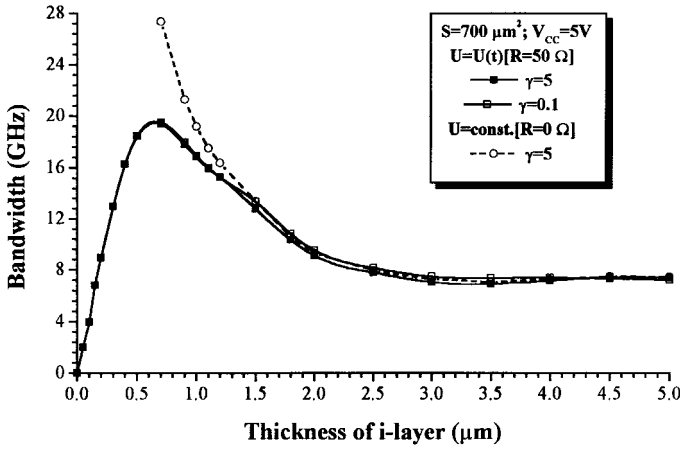


Fig. 2. The bandwidth versus thickness of i-layer of the p-i-n photodiode dependence, in the case of bias voltage  $V_{CC} = 5$  V, active area  $S = 700 \mu\text{m}^2$ , for two different energies of incident excitation  $W = 0.002$  pJ ( $\gamma = 0.1$ ) and  $W = 0.1$  pJ ( $\gamma = 5$ ), together with the transit time limited bandwidth for  $\gamma = 5$ .

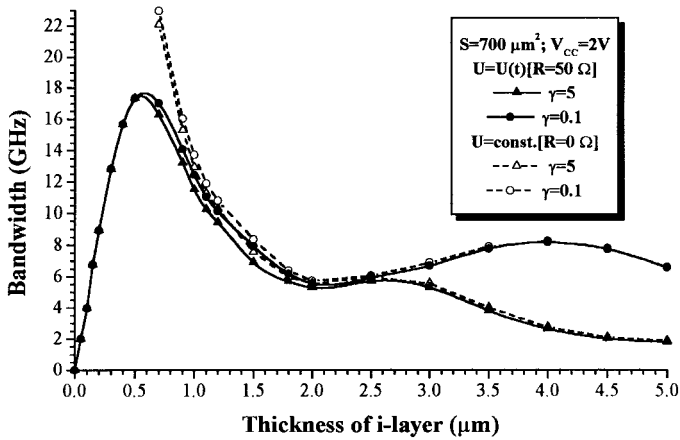


Fig. 3. Same as in Fig. 2, but for bias voltage  $V_{CC} = 2$  V and both of the transit time limited bandwidths.

dependence of the bandwidth on the absorption layer depth has a maximum. The bandwidth is determined by two main factors. For submicron dimensions of the absorption layer the bandwidth is determined by the photodiode RC-constant. For micron dimensions the bandwidth depends on carriers transit times. The carrier transit time increases with the absorption layer depth and the bandwidth thus decreases. The same conclusions were presented in [2] and [9].

However, some new results are presented in Fig. 3. It gives the dependence of the bandwidth on the depth of the absorption layer of the p-i-n photodiode at the bias voltage  $V_{CC} = 2$  V, active area  $S = 700 \mu\text{m}^2$  for two energies of the incident excitation (same as in Fig. 2), together with the transit time limited bandwidth. One should note the different behavior for  $\gamma = 0.1$  and  $\gamma = 5$  cases. For smaller thicknesses of the i-layer the curves almost coincide, but differences appear for thicker layers. A prominent second maximum on the  $\gamma = 0.1$  line is apparent, i.e., the transit time limited bandwidth, for  $V_{CC} = 2$  V and  $\gamma = 0.1$ , is not monotonously decreasing. This differs from the results presented in [2] and [9], because carriers do not travel with the saturation velocity during the

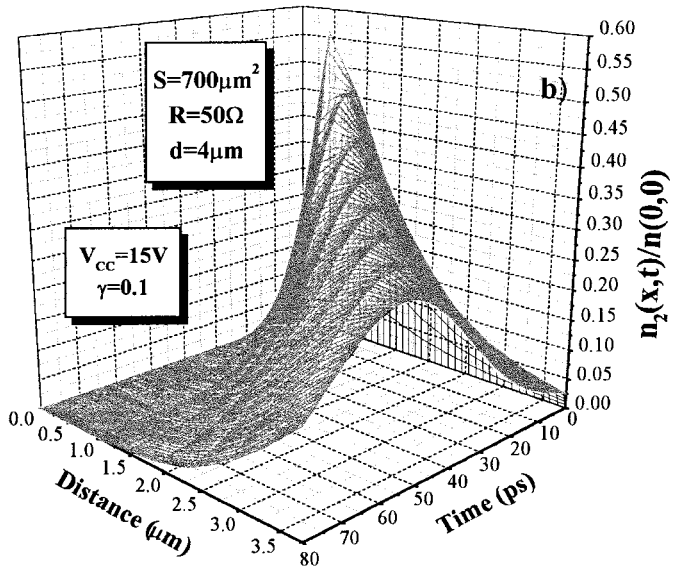
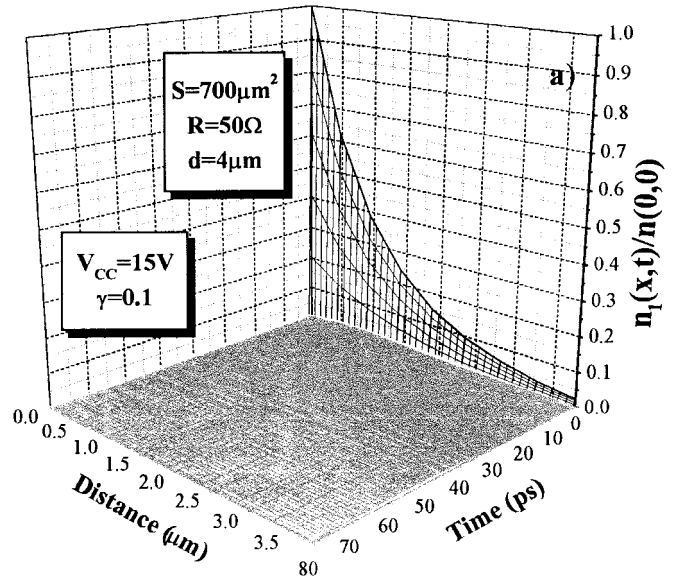


Fig. 4. (a) The profiles of normalized electron concentration in the central valley and (b) the satellite valleys at bias voltage  $V_{CC} = 15$  V, excitation level  $\gamma = 0.1$ , active area  $S = 700 \mu\text{m}^2$  and fixed thickness of the i-layer  $d = 4 \mu\text{m}$ .

transit in the case of small bias voltage  $V_{CC} = 2$  V. This second maximum can be explained within the two-valley model of the absorption layer semiconductor. The transport of generated electrons in GaAs depends significantly on the intervalley transfer between the central ( $\Gamma$ ) and the satellite valleys ( $X$  and  $L$ ). The mobility of electrons in the central valley is larger than in the satellite valleys. At large bias voltages ( $V_{CC} \geq 5$  V), all the electrons accumulate in the satellite valleys, so the transport is slowed down (normalized electron concentrations in the central and the satellite valleys of such a case are respectively given in Fig. 4(a) and (b), for bias voltage  $V_{CC} = 15$  V, excitation level  $\gamma = 0.1$ , active area  $S = 700 \mu\text{m}^2$  and absorption layer thickness  $d = 4 \mu\text{m}$ ). There is a prominent influence of strong electric field here. The electron transport is essentially constrained to the satellite valleys, so the bandwidth is low. The opposite

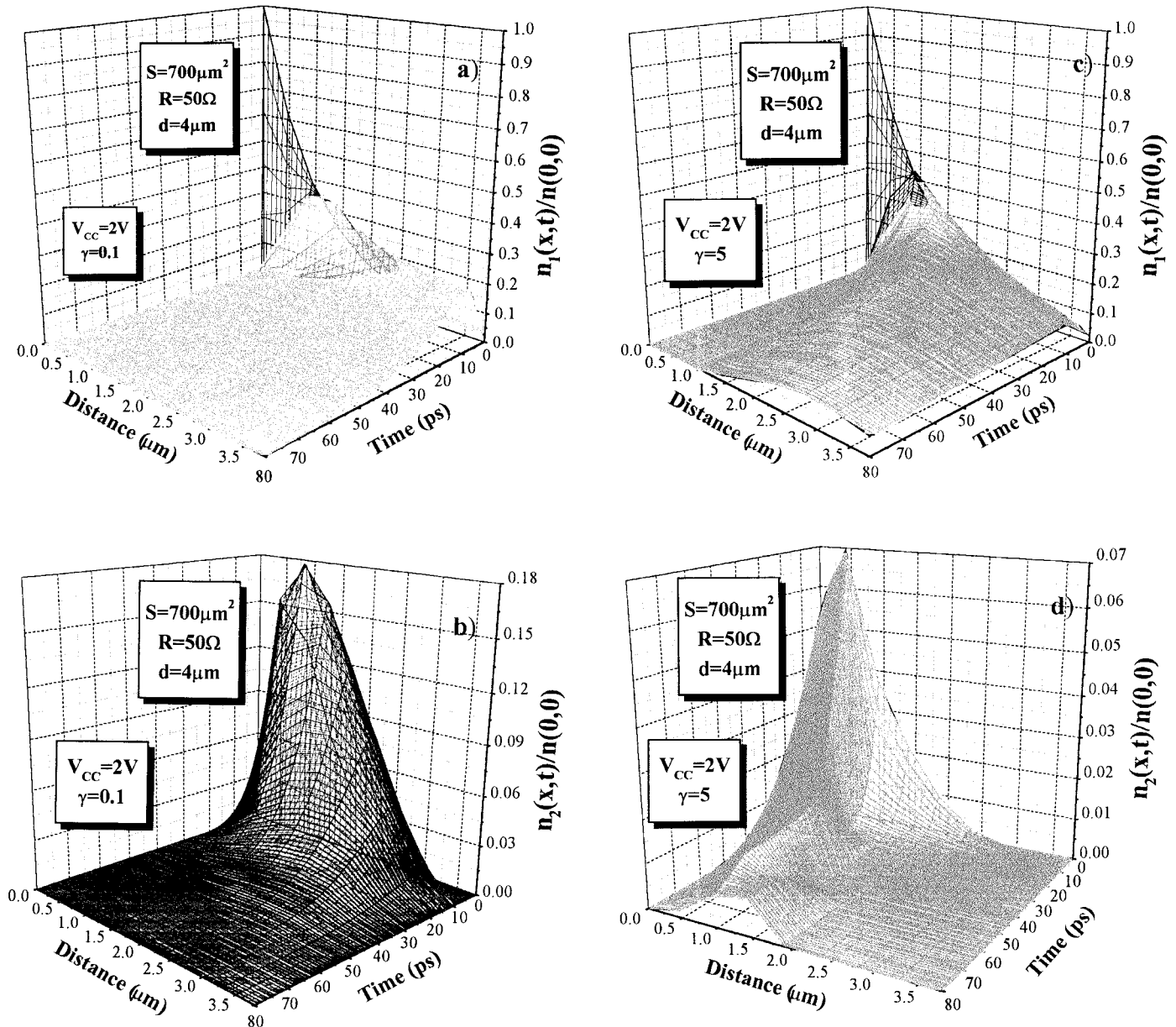


Fig. 5. Same as in Fig. 4(a) and (b), but for bias voltage  $V_{CC} = 2$  V and excitation levels  $\gamma = 0.1$  (a), (b) and  $\gamma = 5$  (c), (d).

case is the electron transport shown in Fig. 5(a) and (b) for  $V_{CC} = 2$  V and  $\gamma = 0.1$ . More electrons here belong to the central valley which implies a faster transport, so the bandwidth is higher. At a low bias voltage of  $V_{CC} = 2$  V and a larger thickness of the absorption layer the electric field is substantially lower, and electrons appear in both valleys in approximately equal amounts [Fig. 5(a) and (b)]. Fig. 5(a) and (c) depicts the normalized electron concentration in the central valley and Fig. 5(b) and (d) in the satellite valleys for the two cases ( $V_{CC} = 2$  V;  $\gamma = 0.1$  and  $\gamma = 5$ , respectively) with the absorption layer thickness of  $d = 4$   $\mu\text{m}$  and active area of  $S = 700$   $\mu\text{m}^2$ . For  $\gamma = 0.1$  electron concentrations in the central and the satellite valleys are much smaller than for  $\gamma = 5$ , so it takes less time to empty all the valleys in the former case. This implies a faster response and a larger bandwidth. The electron concentrations for  $\gamma = 0.1$  becomes

zero after 70 ps, but for  $\gamma = 5$  it does not. The phenomenon of the second maximum is a consequence of tradeoff between absorption layer thickness and noticeable nonstationary effects of two-valley electrons transport. The maximum appears on the curve for  $V_{CC} = 2$  V and  $\gamma = 0.1$  at a thickness of  $d = 4$   $\mu\text{m}$ .

Our model gives a new phenomenon of bandwidth inversion for large thickness of the i-layer, as shown in Fig. 6, depicting the bandwidth versus the absorption layer depth dependence for  $\gamma = 0.1$ ,  $S = 700$   $\mu\text{m}^2$  at four different bias voltages, together with the transit time limited bandwidths. For smaller thickness of the absorption layer the results as given are indeed expected, but for larger thickness the presented results are new. We found that for thicker absorption layers the bandwidth decreases as the bias voltage increases, the phenomenon of the bandwidth inversion, appearing as a consequence of the intervalley transfer (Figs. 4 and 5).

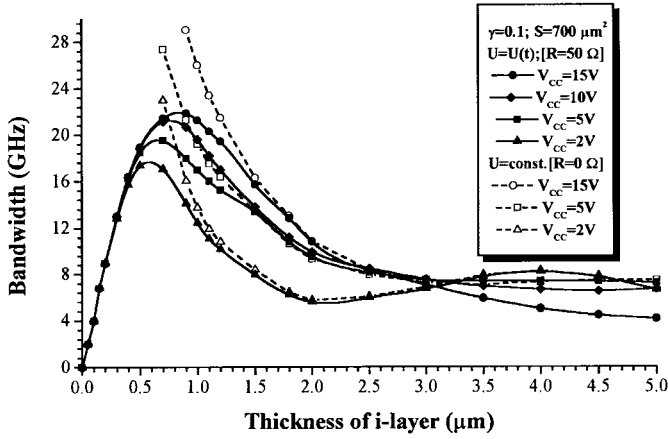


Fig. 6. The bandwidth versus the i-layer thickness dependence for excitation level  $\gamma = 0.1$ , active area  $S = 700 \mu\text{m}^2$  and bias voltages  $V_{CC} = 2 \text{ V}$ ,  $V_{CC} = 5 \text{ V}$ ,  $V_{CC} = 10 \text{ V}$ , and  $V_{CC} = 15 \text{ V}$ , together with the transit time limited bandwidths.

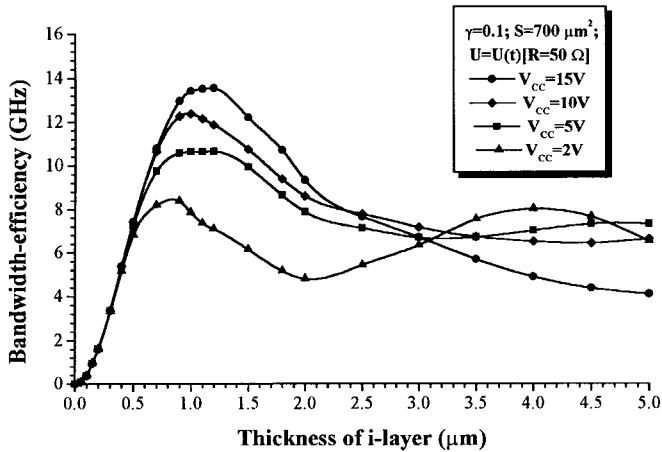


Fig. 7. The bandwidth-efficiency product versus the i-layer thickness dependence for the excitation level  $\gamma = 0.1$  active area  $S = 700 \mu\text{m}^2$  and bias voltages  $V_{CC} = 2 \text{ V}$ ,  $V_{CC} = 5 \text{ V}$ ,  $V_{CC} = 10 \text{ V}$ , and  $V_{CC} = 15 \text{ V}$ .

To complete our considerations we presented in Fig. 7 the bandwidth-quantum efficiency product versus the absorption layer thickness dependence for different bias voltages ( $\gamma = 0.1$  and  $S = 700 \mu\text{m}^2$ ). It is clear from Figs. 6 and 7 that the maxima of the bandwidth and of the bandwidth-efficiency product are higher and slightly moved toward larger thicknesses of the i-layer for larger bias voltages. The bandwidth-efficiency product is more sensitive because the quantum efficiency is larger for larger thickness of the i-layer. A higher value of the maximum at larger bias is simply due to a larger electric field. Location of the maximum is defined by trade-off between the RC-limited bandwidth and the transit time limited bandwidth. The RC-limited bandwidth is constant for a fixed active area, but transit time limited bandwidth is higher as the bias increases in the range of smaller i-layer thicknesses (0.1–3  $\mu\text{m}$ ). It implies that the maximum moves toward larger values of the i-layer thickness at higher bias voltages.

Optimal thickness of the i-layer (location of the maximum) is shown in Fig. 8 for maximal bandwidth and the bandwidth-efficiency product ( $\gamma = 0.1$  and  $S = 700 \mu\text{m}^2$ ). A slight increase of the optimal thickness with bias is clearly visible.

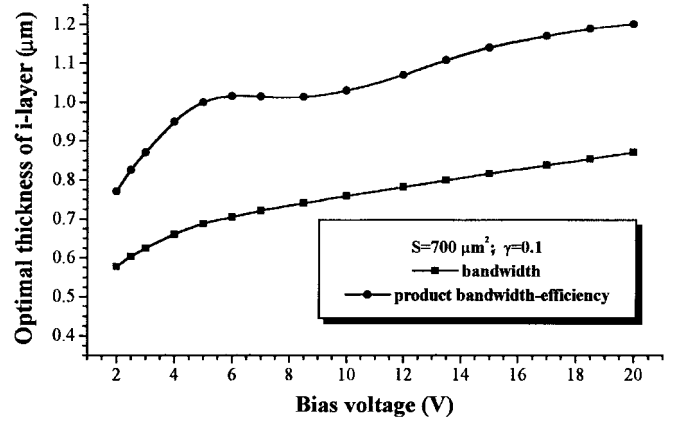


Fig. 8. The optimal thickness of the i-layer versus the bias voltage for the maximal bandwidth and the bandwidth-efficiency product, for excitation level  $\gamma = 0.1$  and active area  $S = 700 \mu\text{m}^2$ .

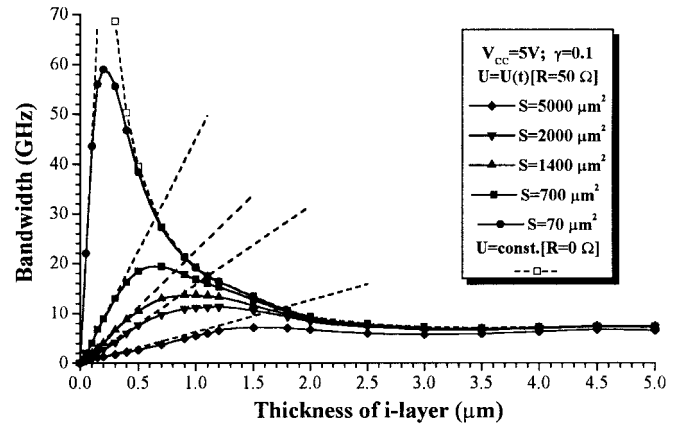


Fig. 9. The bandwidth versus the i-layer thickness dependence for the bias voltage  $V_{CC} = 5 \text{ V}$ , excitation level  $\gamma = 0.1$  and five different values of active area  $S = 70 \mu\text{m}^2$ ,  $S = 700 \mu\text{m}^2$ ,  $S = 1400 \mu\text{m}^2$ ,  $S = 2000 \mu\text{m}^2$ , and  $S = 5000 \mu\text{m}^2$ , together with the RC-limited bandwidths and transit time limited bandwidth.

For the maximal bandwidth, the dependence is almost linear for bias higher than approximately 7 V. For the bandwidth-efficiency product, this dependence has a slight saturation between 6 and 9 V.

Since the value of the maximum and its position both depend on the tradeoff between the RC-limited bandwidth and the transit time limited bandwidth, which depend on the active area and the bias voltage, respectively, we further investigate the dependence of bandwidth on the active area. In Figs. 9 and 10, we give the bandwidth and the bandwidth-efficiency product versus the absorption layer thickness dependencies, for  $\gamma = 0.1$ ,  $V_{CC} = 5 \text{ V}$  and five different values of the active area, respectively. In Fig. 9, the RC-limited bandwidths and the transit time limited bandwidth are given. The RC-limited bandwidths are represented by straight lines with slopes depending on the active area. These straight lines are described by

$$f_B = \frac{1}{2\pi RC} = \frac{d}{2\pi\epsilon RS} \quad (20)$$

where  $f_B$  is the bandwidth,  $C = \epsilon S/d$  is the capacitance and  $S$  is the active area. The transit time limited bandwidth

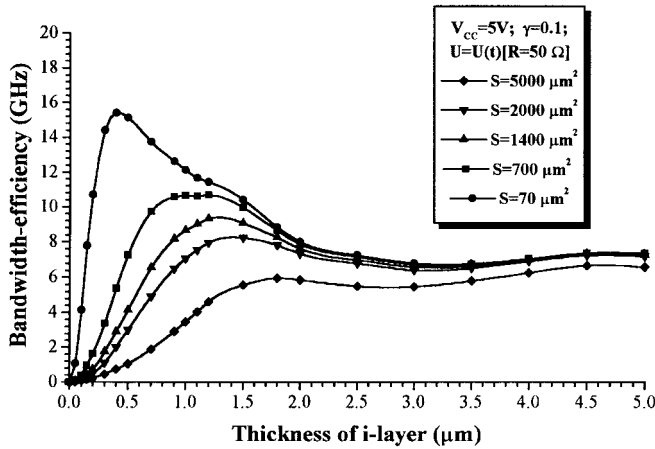


Fig. 10. The bandwidth-efficiency product versus the i-layer thickness dependence for the bias voltage  $V_{CC} = 5$  V, excitation level  $\gamma = 0.1$  and five different values of active area  $S = 70 \mu m^2$ ,  $S = 700 \mu m^2$ ,  $S = 1400 \mu m^2$ ,  $S = 2000 \mu m^2$ , and  $S = 5000 \mu m^2$ .

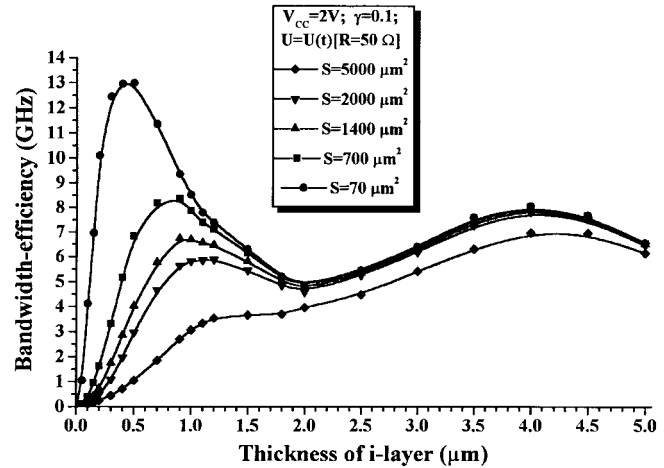


Fig. 12. The bandwidth-efficiency product versus the i-layer thickness dependence for bias voltage  $V_{CC} = 2$  V, excitation level  $\gamma = 0.1$  and five different values of active area  $S = 70 \mu m^2$ ,  $S = 700 \mu m^2$ ,  $S = 1400 \mu m^2$ ,  $S = 2000 \mu m^2$ , and  $S = 5000 \mu m^2$ .

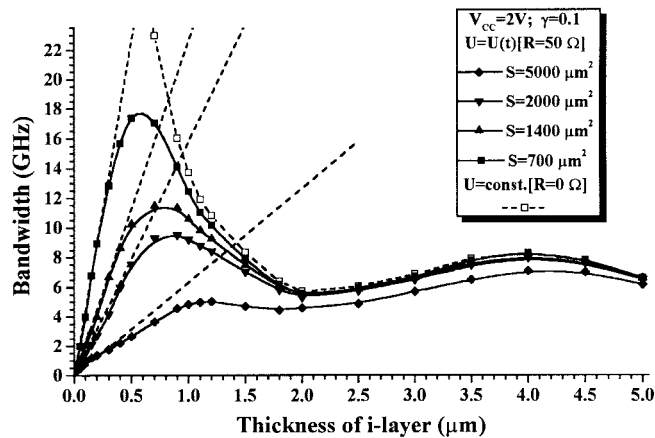


Fig. 11. The bandwidth versus the i-layer thickness dependence for the bias voltage  $V_{CC} = 2$  V, excitation level  $\gamma = 0.1$  and four different values of active area  $S = 700 \mu m^2$ ,  $S = 1400 \mu m^2$ ,  $S = 2000 \mu m^2$ , and  $S = 5000 \mu m^2$ , together with the RC-limited bandwidths and transit time limited bandwidth.

was calculated for  $V_{CC} = 5$  V and  $\gamma = 0.1$ . It is obvious that the lines of RC-limited bandwidth completely describe the full bandwidth for small dimensions of the absorption layer. These results show that the model of the p-i-n photodiode used in [3] does not properly include the influence of the RC-constant on the bandwidth. Qualitative agreement between the models presented here and in [3] is observed only for the transit time limited bandwidth. Agreement between this model and similar ones in [2] and [9] is obvious. It is apparent that the maxima of the bandwidth and the bandwidth-efficiency product strongly depend on the device area. For larger active areas the maximum is smaller and moves toward larger thicknesses of the i-layer. This is a consequence of the fact that the active area influences the RC-limited bandwidth. Now, the transit time limited bandwidth is constant because the bias voltage  $V_{CC} = 5$  V is the same for all the curves in Figs. 9 and 10. The slope of the RC-limited bandwidth is inversely proportional to the active area of p-i-n photodiode, so the maximum is moved toward larger thicknesses of the i-layer for larger active areas, especially the bandwidth-efficiency

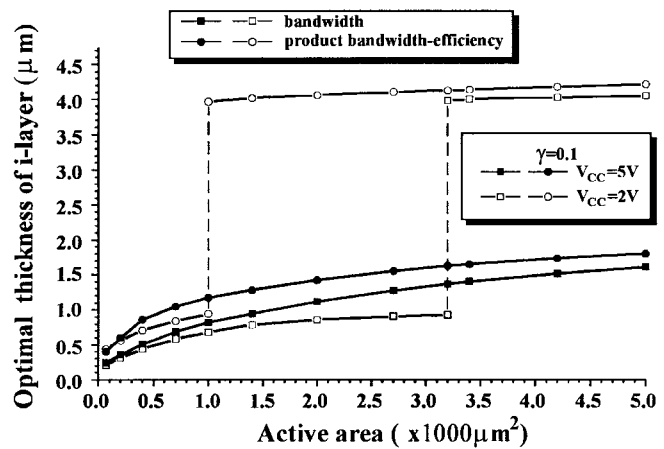


Fig. 13. The optimal thickness of the i-layer versus the active area dependence for the maximal bandwidth and the bandwidth-efficiency product, for bias voltages  $V_{CC} = 2$  V,  $V_{CC} = 5$  V and excitation level  $\gamma = 0.1$ .

product maximum, because quantum efficiency is higher for larger thicknesses. This shift is more prominent than that in Figs. 5 and 7 because the RC-limited bandwidth versus the active area dependence is stronger than the transit time limited bandwidth versus the bias voltage dependence. We conclude that for extremely large active area the bandwidth versus the i-layer thickness dependence cannot have a prominent maximum because the RC-limited bandwidth would intercept this dependence in the range of saturation ( $d \in (3, 5) \mu m$ ). The same is true for the bandwidth-efficiency product versus the i-layer thickness dependence, but for smaller values of the active area. In case of low bias voltages ( $V_{CC} = 2$  V) the bandwidth and the bandwidth-efficiency product versus the absorption layer thickness dependencies are presented in Figs. 11 and 12, respectively. With the increase of active area, the bandwidth maximum, which has appeared due to tradeoff between the RC-limited and the transit time limited bandwidth, decreases, while the second maximum, which has appeared due to nonstationary electron transport remains practically unchanged. Therefore, the optimal absorption layer

thickness slowly increases with the increase of active area, until the active area reaches a critical value, for which the first maximum is lower than the second. After that, a further increase of active area causes a rapid increase in the optimal thickness, from submicron to micron dimensions (about 4  $\mu\text{m}$ ), the optimal thickness remaining unchanged regardless of further area increase. This should be obvious from Fig. 13, which depicts the optimal thickness of the i-layer as a function of the active area for maximal bandwidth and the bandwidth-efficiency product ( $V_{\text{CC}} = 2 \text{ V}$ ,  $V_{\text{CC}} = 5 \text{ V}$  and  $\gamma = 0.1$ ).

## V. CONCLUSION

From the above investigation we have derived the following conclusions.

- By applying the complete phenomenological model of transport equations, we have shown that for the optimal thickness of the absorption layer of GaAs p-i-n photodiode the bandwidth has a maximum which, for bias voltages from 2 V to 15 V, increases from 17 GHz to 23 GHz. At lower bias voltages (about 2 V), there is a second maximum, too. It appears for thickness of the absorption layer which is considerably larger than optimal ( $d = 4 \mu\text{m}$ ). If the active area is large enough, this maximum will be the global maximum. The appearance of the second maximum (9 GHz) is explained by a prominent intervalley electron transfer.
- For thick absorption layers (3–5  $\mu\text{m}$ ) the increase of the bias voltage causes the decrease of the bandwidth from 9 to 5 GHz, while for thin layers (0.1–2.5  $\mu\text{m}$ ) the bandwidth increases from 17 to 23 GHz. This may be called the bandwidth inversion.
- At larger bias voltages ( $V_{\text{CC}} \geq 5 \text{ V}$ ) the bandwidth maximum is higher and slightly moved toward larger values of the absorption layer thickness. Thus, the optimal thickness increases with the bias voltage from 0.6  $\mu\text{m}$  to 0.8  $\mu\text{m}$ .
- If the RC-constant increases, for higher bias voltages ( $V_{\text{CC}} \geq 5 \text{ V}$ ) the bandwidth maximum becomes lower and moves toward larger absorption layer depths. Thus, the optimal thickness increases from 0.2  $\mu\text{m}$  to 1.6  $\mu\text{m}$  when the photodiode area increases from 100  $\mu\text{m}^2$  to 5000  $\mu\text{m}^2$ . Optimal thickness is determined by the  $RS$  product.
- If a p-i-n photodiode made of a two-valley semiconductor (GaAs) with a large active area ( $S \geq 3200 \mu\text{m}^2$ ) is operated under low bias conditions (approx. 2 V), the optimal thickness of the i-layer is 4  $\mu\text{m}$  and does not depend on the RC-constant. This is very important for applications where a reduced dissipation in the semiconductor circuitry is of prime importance.
- The same conclusions are also valid for the bandwidth-efficiency product.

The complete phenomenological model is one of the best optimization tools presently available, because it can handle a wide range of p-i-n photodiode operating conditions with submicron and micron dimensions of the i-layer (device active area and load resistance, bias voltage and the incident pulse excitation parameters).

## REFERENCES

- [1] G. Lucovsky, R. F. Schwarz, and R. B. Emmons, "Transit-time consideration in  $P$ - $I$ - $N$  diodes," *J. Appl. Phys.*, vol. 35, no. 3, pp. 622–628, 1964.
- [2] J. E. Bowers and C. A. Burrus, "Ultrawide-band long-wavelength  $p$ - $i$ - $n$  photodetectors," *J. Lightwave Technol.*, vol. LT-5, pp. 1339–1350, Oct. 1987.
- [3] R. Sabella and S. Merli, "Analysis of InGaAs  $p$ - $i$ - $n$  photodiode frequency response," *IEEE J. Quantum Electron.*, vol. 29, pp. 906–916, Mar. 1993.
- [4] M. Dentan and B. de Cremoux, "Numerical simulation of the nonlinear response of a  $p$ - $i$ - $n$  photodiode under high illumination," *J. Lightwave Technol.*, vol. 8, pp. 1137–1144, Aug. 1990.
- [5] J. B. Radunović and D. M. Gvozdić, "Nonstationary and nonlinear response of a  $p$ - $i$ - $n$  photodiode made of a two-valley semiconductor," *IEEE Trans. Electron Devices*, vol. 40, pp. 1238–1244, July 1993.
- [6] R. Stenzel, H. Elschner, and R. Spallek, "Numerical simulation of GaAs MESFET's including velocity overshoot," *Solid-State Electron.*, vol. 30, no. 8, pp. 873–877, 1987.
- [7] J. Soole and H. Schumacher, "InGaAs metal-semiconductor-metal photodetector for long wavelength optical communications," *IEEE Trans. Electron Devices*, vol. 27, pp. 737–752, 1991.
- [8] G. Strang, *Introduction to Applied Mathematics*. New York: Wellesley Cambridge, 1986.
- [9] Y. Leblebici, M. S. Ünlü, S.-M. Kang, and B. M. Onat, "Transient simulation of heterojunction photodiodes—Part II: Analysis of resonant cavity enhanced photodetectors," *J. Lightwave Technol.*, vol. 13, pp. 406–415, Mar. 1995.



**Petar S. Matavulj** was born in Gradiška, Srpska Republic, in 1971. He received the B.S. and the M.S. degrees in electrical engineering from Belgrade University, Belgrade, Yugoslavia, in 1994 and 1997, respectively. He is currently working toward the Ph.D. degree in electrical engineering at Belgrade University.

In 1994, he joined the Faculty of Electrical Engineering, University of Belgrade, where he is now an Assistant of Physical Electronics. His research interests are the modeling, simulation, and characterization of high-speed optoelectronic devices and fiber optics sensors.

He is a student member of the IEEE Laser and Electro-Optics Society and IEEE Electron Devices Society.



**Dejan M. Gvozdić** was born in Boljevac, Serbia, Yugoslavia, in 1964. He received the M.S. and Ph.D. degrees in electrical engineering from Belgrade University, Belgrade, Yugoslavia, in 1992 and 1995, respectively.

In 1989, he joined the Faculty of Electrical Engineering, University of Belgrade, where he is now an Assistant Professor of Solid State Electronics and Integrated Optics. His present research interests are modeling and simulation of optoelectronic devices, waveguided-coupled and resonant-cavity enhanced

photodetectors.



**Jovan B. Radunović** was born in Priština, Serbia, Yugoslavia, in 1949. He received the M.S. and Ph.D. degrees in electrical engineering from Belgrade University, Belgrade, Yugoslavia, in 1977 and 1984, respectively.

In 1974, he joined the Faculty of Electrical Engineering, University of Belgrade, where he is now a Professor of Physical Electronics. His research areas include fundamental studies of kinetic fluctuations in semiconductors, electron transport in semiconductors, and modeling and simulation of high-speed

semiconductor devices.